Structure of *Arabidopsis* Dehydroquinate Dehydratase-Shikimate Dehydrogenase and Implications for Metabolic Channeling in the Shikimate Pathway[†,‡]

Sasha Anna Singh and Dinesh Christendat*

Department of Botany, University of Toronto, 25 Willcocks Street, Toronto, ON M5S 3B2, Canada

Received February 21, 2006; Revised Manuscript Received April 25, 2006

ABSTRACT: The bifunctional enzyme dehydroquinate dehydratase-shikimate dehydrogenase (DHQ-SDH) catalyzes the dehydration of dehydroquinate to dehydroshikimate and the reduction of dehydroshikimate to shikimate in the shikimate pathway. We report the first crystal structure of *Arabidopsis* DHQ-SDH with shikimate bound at the SDH site and tartrate at the DHQ site. The interactions observed in the DHQ−tartrate complex reveal a conserved mode for substrate binding between the plant and microbial DHQ dehydratase family of enzymes. The SDH−shikimate complex provides the first direct evidence of the role of active site residues in the catalytic mechanism. Site-directed mutagenesis and mechanistic analysis revealed that Asp 423 and Lys 385 are key catalytic groups and Ser 336 is a key binding group. The arrangement of the two functional domains reveals that the control of metabolic flux through the shikimate pathway is achieved by increasing the effective concentration of dehydroshikimate through the proximity of the two sites.

The shikimate pathway is involved in the biosynthesis of the aromatic amino acids, folates, vitamins, quinones, and a variety of other aromatic compounds in bacteria, plants, fungi, and apicomplexa parasites. Some of the aromatic compounds are essential for the survival of these organisms; as a result, the shikimate pathway has been an attractive target for the design of antimicrobial and herbicidal agents. The importance of this pathway in biotechnology has been exemplified by glyphosate, a herbicide which targets EPSP[1] synthase (*1*). However, the emergence of glyphosate-resistant plants and microbes (*2*, *3*) demonstrates the need to target other enzymes of the pathway.

The shikimate pathway consists of seven enzymatic steps which ends with the formation of chorismate, the branch point precursor for the biosynthesis of the aromatic compounds (*4*−*6*). The organization of the seven enzymes is markedly different among the three kingdoms. In most prokaryotes, the seven enzymatic reactions are catalyzed by monofunctional enzymes; in fungi, reactions 2−6 are catalyzed by the multifunctional AROM complex, and in plants, a bifunctional dehydroquinate dehydratase-shikimate dehydrogenase (DHQ-SDH) catalyzes the third and fourth reactions of the pathway. An elaborate study of the shikimate pathway in plants is lacking. The structures of the plant enzymes have not been determined, and limited mechanistic information for these enzymes is available. To date, the annotation of the *Arabidopsis thaliana* shikimate pathway enzymes has been based solely on bioinformatics analyses.

The enzyme dehydroquinate dehydratase (DHQ, EC 4.2.1.10) catalyzes the dehydration of 3-dehydroquinate to 3-dehydroshikimate (Scheme 1). Two types of DHQs have been characterized. Type I and II enzymes catalyze the syn and anti elimination of water, respectively. The structures of both types have been determined from microbes and fungi (*7*−*10*). Type I is characterized as an $(\alpha/\beta)_8$ or TIM barrel, and type II is characterized as a mixed α/β possessing a central five-stranded parallel β sheet flanked by four α helices, reminiscent of a flavodoxin fold (*7*, *8*).

The enzyme shikimate dehydrogenase (SDH, EC 1.1.1.25) catalyzes the reversible reduction of 3-dehydroshikimate to shikimate (Scheme 1). Three classes of SDHs have been identified on the basis of phylogenetic and biochemical analyses: shikimate dehydrogenase (AroE), shikimate/quinate dehydrogenase (YdiB), and shikimate dehydrogenase-like (SDH-L) (*11*, *12*). All three classes of SDH can catalyze the oxidation of shikimate in the presence of $NADP^+$, albeit with varying catalytic efficiencies (*11*, *12*). The shikimate/quinate dehydrogenase enzyme accepts quinate as its natural substrate, whereas that of the SDH-L enzyme has not yet been determined. The crystal structures of all three classes of SDH have been determined (*11*−*14*). Although these three classes of SDH have different biochemical functions, their three-dimensional structures are highly conserved (*11*).

[†] This research was supported by a grant from the Natural Science and Engineering Research Council (NSERC) of Canada to D.C. and a major facilities access grant from the Canadian Institute for Health Research (CIHR) and NSERC to operate beamline XBC at the National Synchrotron Light Source. S.A.S. was supported in part by the Ontario Graduate Scholarship in Science and Technology (OGSST) program and a University of Toronto Fellowship (UTF).

[‡] The atomic coordinates and structure factors for DHQ-SDH (entry 2GPT) have been deposited in the Protein Data Bank, Research Collaboratory for Structural Bioinformatics, Rutgers University, New Brunswick, NJ (http://www.rcsb.org/).

* To whom correspondence should be addressed. E-mail: dinesh.christendat@utoronto.ca. Phone: (416) 946-8373.

[1] Abbreviations: DAHP, 3-deoxy-D-*arabino*-heptulosonate 7-phosphate; EPSP, 5-enolpyruvylshikimate 3-phosphate; DHQ, dehydroquinate dehydratase; SDH, shikimate dehydrogenase; NADP(H), nicotinamide adenine dinucleotide diphosphate; SDH-L, shikimate dehydrogenase-like; IPTG, isopropyl β-D-thiogalactopyranosid; SeMet, selenomethionine.

10.1021/bi060366+ CCC: $33.50
Published on Web 06/01/2006

Scheme 1: Reactions Catalyzed by *A. thaliana* DHQ-SDH, the Dehydration of Dehydroquinate (DQ) to Dehydroshikimate (DHS) Followed by the Reduction to Shikimate (SK)

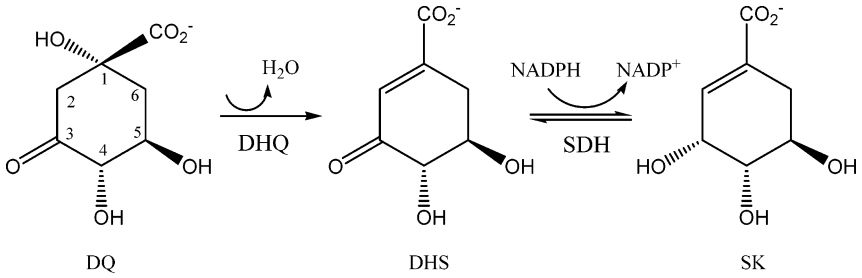

DQ DHS SK

Bifunctional enzymes play important roles in regulating the partition of metabolites at branch points in metabolic pathways to ensure sufficient production of a desired compound(s). Annotation of the *A. thaliana* genome identified only 23 bifunctional enzymes; a similar number is also thought to exist in other plants (*15*). In plants, DHQ-SDH is the only bifunctional shikimate pathway enzyme. DHQ-SDH is found at the branch point for quinate biosynthesis; dehydroquinate and dehydroshikimate, the substrates for DHQ and SDH, respectively, can be partitioned toward quinate metabolism (Figure 1). In plants, quinate is a precursor for chlorogenic acids which serve as antiherbivory compounds as well as antioxidants in animal diets (*16*, *17*). Quinate (and shikimate)-*p*-coumaryl esters have also been identified as intermediates in lignin biosynthesis (*18*). Substrate channeling from the DHQ to SDH site will ensure a constant flux through the shikimate pathway for chorismate biosynthesis.

This study is the first to report structural and kinetic analyses on the *A. thaliana* bifunctional enzyme, DHQ-SDH and, moreover, the structure of the DHQ−tartrate−SDH−shikimate cocomplexes. Furthermore, the superimposition of the SDH domain of *A. thaliana* with that of AroE-$NADP^+$ from *Thermus thermophilus* produces the first structure of the SDH ternary complex. The crystal structure of DHQ-SDH is also important for understanding the mode of substrate channeling between the DHQ and SDH active sites. Furthermore, the crystal structure of this bifunctional enzyme with its substrate and substrate analogue advances our understanding of drug and herbicide design against the shikimate pathway.

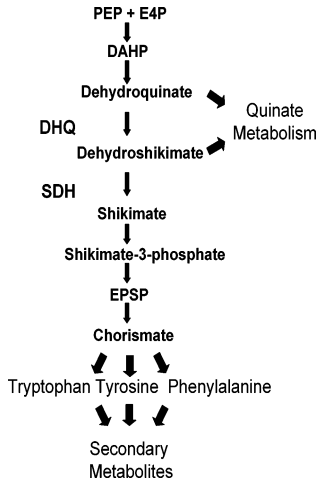

FIGURE 1: Metabolite partitioning from the shikimate pathway. The shikimate pathway commences with the condensation of phosphoenolpyruvate (PEP) with erythrose 6-phosphate (E4P) and ends with the formation of chorismate. Chorismate, through a series of enzymatic reactions, can be converted to tryptophan, tyrosine, or phenylalanine. Dehydroquinate dehydratase (DHQ) and shikimate dehydrogenase (SDH) catalyze steps 3 and 4, respectively, in the shikimate pathway. Intermediates dehydroquinate and dehydroshikimate can be partitioned toward quinate metabolism.

Table 1: Forward Primers Used To Generate Active Site Mutants

mutant	forward primer[a]
S336A	gcctgtcagccac***gcc***aaatcacctattgttc
S338A	gccacagcaaa***gcc***cctattgttcacaatcaagc
K385N	gctgtacaattccgcac***aac***gaagctgcattgcaatg
K385A	gctgtacaattccgcac***gca***gaagctgcattgcaatg
D423N	gggttacaacaca***aac***tgtattggttccatttctgc
D423A	gggttacaacaca***gca***tgtattggttccatttctgc
Y550F	gtctttgatgcggta***ttc***actccgagaatcacc
Y550A	gtctttgatgcggta***gcc***actccgagaatcacc

[a] Italicized bases indicate the substituted codon.

EXPERIMENTAL PROCEDURES

Chemicals and Reagents. All reagents are molecular biology grade and were purchased from Sigma, Bioshop, or BDH. Oligonucleotides for cloning and polymerase chain reaction (PCR) mutagenesis experiments were purchased from Sigma Genosys.

Cloning and Site-Directed Mutagenesis. The full-length gene At3g06350 encoding DHQ-SDH and expression construct Δ88DHQ-SDH, representing residues 89−603, were PCR amplified from *A. thaliana* cDNA and cloned into a modified pET28 vector at the NdeI and BamHI sites. The modified vector consists of a C-terminal histidine tag. ChloroP (http://www.cbs.dtu.dk/services/ChloroP/) was used to determine the chloroplast transit peptide. Prof (http://www.aber.ac.uk/~phiwww/prof/) was used to determine the boundaries of secondary structures, which subsequently allowed us to design constructs such as Δ88DHQ-SDH, which do not disrupt any secondary structure.

Site-directed mutagenesis was carried out using the QuickChange site-directed mutagenesis kit (Stratagene) where complementary oligonucleotides containing the required mutations for Δ88DHQ-SDH were used (Table 1). The Δ88DHQ-SDH construct in the modified pET28 vector was used as a template, and mutagenesis was completed according to the protocol suggested by Stratagene. The mutants were verified by DNA sequencing.

Expression and Purification. The expression and purification of Δ88DHQ-SDH wild-type and mutant proteins were accomplished as follows: Δ88DHQ-SDH wild-type and mutant recombinants were expressed in *Escherichia coli* strain BL21 Codon+ in 1 L of Luria-Bertani medium supplemented with kanamycin (50 μg/mL) and incubated at

37 °C with shaking until the cultures reached an OD_{600} of 0.6−0.8. The cultures were induced with 0.4 mM isopropyl β-D-thiogalactopyranosid (IPTG) for 3 h at 37 °C and then allowed to grow for an additional 4 h with shaking at 24 °C. Cells were harvested by centrifugation and disrupted by sonication, and the insoluble cellular material was removed by centrifugation. The recombinants were purified from other contaminating proteins using Ni−NTA affinity chromatography. Protein samples for kinetic and CD studies were dialyzed and stored in 10 mM Tris-HCl (pH 7.5), 500 mM NaCl, and 5% glycerol. Protein for crystallization studies was digested with 0.15 mg of TEV protease, per 20 mg of purified protein, for 16 h at 4 °C. The TEV protease and cleaved histidine tags were removed by Ni−NTA chromatography. The purified proteins were dialyzed and stored in buffer containing 10 mM HEPES (pH 7.5) and 500 mM NaCl. All purified proteins were quantified at 280 nm using an extinction coefficient of 40 470 M^{-1} cm^{-1}. Selenomethionine-labeled protein was prepared as follows. Wild-type Δ88DHQ-SDH was expressed in BL21 Codon+ cells in M9 minimal medium containing 0.4% (w/v) glucose as a carbon source. Once the cells reached an OD_{600} of 0.8, a selenomethionine (SeMet) amino acid cocktail (per liter of culture, 60 mg of SeMet, 100 mg of lysine, threonine, and phenylalanine, and 50 mg of leucine, isoleucine, and valine) was added. IPTG induction followed 15 min after addition of the cocktail, and the cells were allowed to grow as described above for the native protein. Protein purification was conducted exactly as described above for the native protein, the exception being that 5 mM β-mercaptoethanol was present in all buffers.

Enzyme Kinetic Assays. The enzymatic activity of the SDH domain of wild-type and mutant Δ88DHQ-SDH recombinants was assayed by monitoring the reduction of $NADP^+$ ($\epsilon = 6220$ M^{-1} cm^{-1}) at 340 nm and 22 °C in the presence of shikimate. Saturation kinetics studies were carried out at pH 8.8. The K_m and V_{max} values were determined by varying the concentrations of either shikimate or $NADP^+$ while keeping the other substrate at saturation; 2 mM shikimate and 1 mM $NADP^+$ were considered saturating for the wild type and most of the mutant enzymes. Mutants Ser336Ala and Ser338Ala were determined to have elevated K_m values as such $NADP^+$ saturation curves were determined at the fixed, nonsaturating concentration of 5 mM shikimate and compared to the equivalent, relative K_m value for the wild type (40% or 250 μM shikimate).

Data Analysis. The kinetic data were fitted to the following rate equations using the computer programs of Cleland or GraFit (*19*). Initial velocity data were obtained by varying the concentration of either shikimate or $NADP^+$ (*A*) and fitted to eq 1 to yield maximal velocity values (*V*) and the Michaelis constant (*K*).

$$v = \frac{VA}{K + A} \tag{1}$$

Circular Dichroism Analysis and Thermal Denaturation of Δ88DHQ-SDH Variants. Wild-type and mutant Δ88DHQ-SDH proteins were dialyzed for a total of 8 h, with two changes of buffer, in 10 mM Tris-HCl (pH 7.5) and 500 mM NaCl. Protein samples with a final concentration of 10 μM (5 μM for Ser338Ala and Tyr550Ala) were prepared by diluting the original stocks with the dialysis buffer. The absorbance spectrum and thermal denaturation profile of each protein were monitored by circular dichroism (CD) using a Jasco J-810 spectropolarimeter. The change in the α-helical signal of the protein at 222 nm (1 nm bandwidth) was recorded as a function of temperature (25−85 °C), with a temperature gradient of 1 °C/min.

The fraction of unfolded protein was calculated at each temperature point with eq 2:

$$F_u = \frac{\theta_i - \theta_t}{\theta_i - \theta_f} \tag{2}$$

where F_u is the fraction of protein unfolded, θ_i is the initial ellipticity, θ_t is the ellipticity at a specific temperature, and θ_f is the final molar ellipticity of the denatured protein. For presenting data, F_u was converted to %U by multiplying F_u by 100.

Gel Filtration. Gel filtration of wild-type Δ88DHQ-SDH (3 mg/mL) was performed with a Superdex 200 prep 16/60 column (GE Healthcare) equilibrated in 10 mM HEPES and 500 mM NaCl using AKTA Explorer (GE Healthcare). A final concentration of 0.4 M potassium sodium tartrate tetrahydrate or 1 mM shikimate was added to the equilibration buffer for dimerization studies. The equivalent concentrations of substrates were also added to the protein sample. The protein standards were bovine serum albumin, ovalbumin, and cytochrome *c*. Chromatography was performed at 4 °C at a flow rate of 0.5 mL/min.

Crystallization Conditions. An initial crystallization condition for the wild-type protein construct, Δ88DHQ-SDH, was obtained with a sparse matrix (Hampton Research Crystal Screen 2) using the vapor diffusion hanging-drop technique. This condition was modified by varying the concentrations of the salts potassium sodium tartrate tetrahydrate and ammonium sulfate. Optimal crystals grew in 0.4 M potassium sodium tartrate tetrahydrate, 0.1 M tri-sodium citrate dihydrate (pH 5.6), and 2.8 M ammonium sulfate using 2 μL of a 1:1 (v/v) protein (10 mg/mL with 1 mM shikimate)/reservoir solution.

Data Collection and Refinement. The X-ray data and refinement statistics for the SeMet and native proteins are presented in Table 2. All X-ray diffraction data were collected at beamline X8-C at the National Synchrotron Light Source (NSLS) (Brookhaven National Laboratory, Upton, NY). The diffraction data were processed and scaled with the HKL2000 software package (*20*). An initial SAD phasing experiment with the Se peak data was conducted with SOLVE to determine the positions of the Se atoms. Further phase improvements were conducted by density modification with RESOLVE (*21, 22*). Automated model building was done with RESOLVE followed by ARP/warp (*23, 24*) which built a total of 418 residues, constituting 80% of the model. The remaining model was manually built with O (*24*), and simulated annealing refinements were carried out with the CNS software package (*25*) and with the Se peak data set. Once R_{free} dropped below 30% for the refined model, the native data set was used for all further energy minimization refinements. Tartrate and shikimate PDB, topology, and parameter files were obtained from the HIC-up server (http://xray.bmc.uu.se/hicup). In the later stages of refinement of the model, tartrate, shikimate and two sulfates were added

Table 2: Summary of X-ray Data Collection and Refinement Statistics

X-ray Data		
	native	peak
space group	$P3_221$	$P3_221$
unit cell (Å^3)	96.9 × 96.9 × 116.2	96.95 × 96.95 × 116.569
resolution (Å)	50−1.95	50−2.2
wavelength (Å)	1.1000	0.9795
total no. of observations	331076	678298
no. of unique observations	46428	36574
redundancy	7.1	7.2
intensity ($I/\sigma\langle I\rangle$)	42.9 (3.3)	31.3 (6)
completeness (%)	99.7 (98.5)	99.3 (96.1)
R_{sym}[a]	0.044 (0.537)	0.066 (0.348)

Summary of SOLVE Statistics	
no. of Se sites located	12/12
SOLVE *Z*-score	80.0

Summary of Refinement Statistics	
R_{factor}[b]	0.229
R_{free}[c]	0.254
no. of protein atoms	3874
no. of water molecules	264
no. of tartrate molecules	1
no. of shikimate molecules	1
no. of sulfate ions	2
rmsd for bond lengths (Å)	0.006
rmsd for bond angles (deg)	1.3
rmsd for dihedrals (deg)	22.5
B-factor (Å^2)	39

[a] $R_{sym} = \sum[(I - \langle I\rangle)^2]/\sum(I)^2$, where I is the observed integrated intensity, $\langle I\rangle$ is the average integrated intensity obtained from multiple measurements, and the summation is over all observed reflections.[b] $R_{factor} = \sum|F_{obs} - F_{calc}|/|F_{obs}|$. [c] R_{free} was calculated using a randomly selected set of reflections (1309 reflections).

which fitted well with the difference electron density. Water was added just before the last three rounds of model rebuilding and energy minimization refinements. Figures were produced with MolScript, Spock, and PyMOL (*26*) (http://quorum.tamu.edu/; http://pymol.sourceforge.net/). The DALI server was used to search for structural homologues of DHQ-SDH. In addition to the coordinates for the bifunctional enzyme, coordinates for DHQ and SDH domains were separately submitted to the DALI server.

RESULTS

DHQ-SDH Construct Design

To obtain a stable and active *A. thaliana* DHQ-SDH enzyme, in addition to the full-length protein, a number of expression constructs without the predicted chloroplast transit peptide were designed. Our best construct, as judged by expression properties, solubility, and stability, was determined to be Δ88DHQ-SDH which lacks the first 88 residues. Enzymatic assay of the Δ88DHQ-SDH demonstrated that this construct produced an active shikimate dehydrogenase, which was used for all subsequent functional, mutagenesis, and crystallization studies.

Summary of Structure Determination

Large, well-ordered protein crystals were obtained for Δ88DHQ-SDH when it was cocrystallized with shikimate under an optimized hanging-drop crystallization condition containing 0.4 mM sodium tartrate tetrahydrate, 0.1 M trisodium citrate dihydrate (pH 5.6), and 2.8 M ammonium sulfate. The Δ88DHQ-SDH crystals belong to space group $P3_221$ and diffracted to 1.95 Å resolution. A total of 12 selenium atoms were determined by SAD phasing with a single Δ88DHQ-SDH molecule in the asymmetric unit. The refined molecule (R_{factor} = 22.3, R_{free} = 25.3) has excellent stereochemistry as judged by a Ramachandran plot, with 90.6% of the residues in the most favored region, 8.8% in the additional allowed region, and 0.7% in the generally allowed region. The final model consists of 524 residues, one shikimate, one tartrate, two sulfate molecules, and 264 water molecules. Residues 436−454, consisting of primarily serines and prolines, are disordered, as judged by the lack of electron density for this region. The Δ88DHQ-SDH structure consists of two functional domains, dehydroquinate dehydratase (DHQ) and shikimate dehydrogenase (SDH), which are structurally distinct, and are separated by helix α9, residues 315−319 (Figure 2A).

Structure Overview of A. thaliana Δ88DHQ-SDH

DHQ Domain. The DHQ domain adopts the TIM $(\alpha/\beta)_8$ barrel with alternating β/α secondary structures (strand order of β1, α1, β2, α2, β3, α3, β4, α4, β5, α5, β6, α6, β7, α7, β8, and α8), typified by this family of dehydratases, and superposes well with the type I DHQ from *Salmonella typhi* (1QFE) (Figure 2C). A tartrate molecule is bound in the active site in the middle of the TIM barrel (Figure 2A,B). The structure lacks an antiparallel β sheet, observed in the *S. typhi* structure, which caps one side of the barrel (Figure 2C). This antiparallel β sheet is formed by N-terminal residues which were removed in the Δ88DHQ-SDH construct.

SDH Domain. SDH contains nucleotide-binding and substrate-binding domains. The nucleotide-binding domain consists of a six-stranded parallel β sheet (strand order of β17, β16, β15, β18, β19, and β20) sandwiched by two helices (α14 and α15) on one face and by helices α17−α19 on the other (Figure 2A). This topology is similar in all classes of the SDH enzyme with a few exceptions. The AroE structures from *T. thermophilus*, *E. coli*, and *Methanococcus jannaschii* all possess a 3_{10} helix in place of helix α18. Moreover, the *E. coli* and *M. jannaschii* structures also lack the equivalent of helix α17 (*11*−*13*).

The substrate binding-domain adopts an α/β sandwich with a six-stranded, mainly parallel β sheet (strand order of β10, β9, β11, β13, β14, and β12), where β13 is antiparallel. This β sheet is flanked by helices α10 and α21 at one end and helices α12 and α13 at the other (Figure 2A). The overall fold of this functional domain is very similar to that observed for other SDH proteins (*11*, *12*) (Figure 2D).

Description and Analysis of DHQ and SDH Active Sites of Δ88DHQ-SDH

DHQ Active Site. In this study, a single tartrate molecule is bound to the dehydroquinate dehydratase active site (Figure 2A,B). Tartrate binds directly in the middle of the α/β barrel and participates in a number of interactions observed similarly for other type I DHQs bound to dehydroshikimate (Figure 3) (*7*, *8*). Arg 279 is conserved in the type I DHQs; it interacts with the C4 carboxylate of tartrate (Figure 3A).

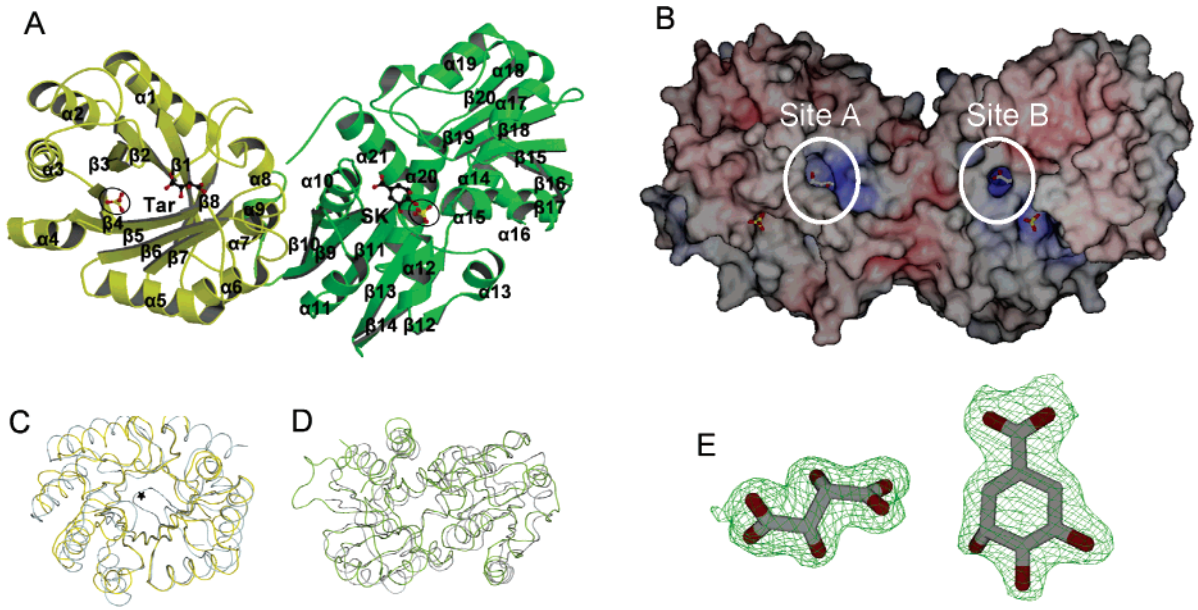

FIGURE 2: *A. thaliana* DHQ-SDH structure. (A) Ribbon diagram of the DHQ (yellow) and SDH (green) domains bound with tartrate (Tar) and shikimate (SK) in the active sites. (B) Electrostatic surface potential of DHQ-SDH showing the relative positions of the DHQ (site A) and SDH (site B) active sites. (C) Superimposition of the *A. thaliana* DHQ domain (yellow) with that of the *S. typhi* structure (cyan). The star identifies the N-terminal β sheet which is present at the base of the *S. typhi* barrel but absent in the *A. thaliana* structure. (D) Superimposition of the *A. thaliana* SDH domain with that of *T. thermophilus* (gray). (E) Composite omit maps of tartrate (left) and shikimate at the 1σ level. Sulfate molecules are circled. α denotes alpha helix and β beta strand.

An analogous interaction is observed at the C1 carboxylate of dehydroshikimate with the *S. typhi* DHQ (Figure 3B). Glu 124, Arg 126, and Asp 128 together with the conserved His 214 and Lys 241 participate in a hydrogen bonding network with the C1 carboxylate of tartrate. His 214 and Lys 241 play important roles in the catalytic mechanism. Lys 241 forms the Schiff base intermediate, and His 214 functions as the catalytic base (*27*−*29*). Phe 291 stacks against the tartrate carbon backbone in a manner analogous to the stacking against the dehydroshikimate ring observed in *S. typhi*. Leu 269 and Met 271 are also in the proximity of tartrate; two methionines are found at similar positions in the *S. typhi* DHQ structure (Figure 3).

A comparison of the active site alignments of the *A. thaliana* DHQ with the *S. typhi* enzyme revealed that the key active site residues are conserved. On the basis of this observation, we propose that these enzymes share a similar catalytic mechanism. In *A. thaliana* DHQ, Arg 279 functions as a key binding group and Lys 241 and His 214 are catalytic groups. Lys 241 forms a Schiff base intermediate, and His 214 functions as the catalytic base and modulates the formation and breakdown of the Schiff base intermediate. This dual role of His 214 is important for maintaining the syn stereochemistry of the dehydration reaction.

SDH Active Site. The substrate binding site is formed predominantly by helices α14 and α20 and strands β9 and β11. Shikimate participates in a number of key interactions which are important either for binding and positioning of the substrate or for catalysis. One set of interactions involves residues Ser 336, Ser 338, and Tyr 550 which bind the C1 carboxylate in a trigonal arrangement (Figure 4). In addition, Asn 406 interacts with the C4 hydroxyl, and Gln 578 and Gln 582 are within hydrogen bonding distance of the C5 hydroxyl and may help to bind and orient the substrate. Thr 407 and Thr 421 which are located further inside the substrate binding pocket conformationally orient residues Asn 406, Gln 578, and Gln 582. We speculated that residues within hydrogen bonding distance of the C3 hydroxyl play a role in catalysis. Lys 385 and Asp 423 meet such criteria (Figure 4).

Superimposition of the *A. thaliana* SDH with the *T. thermophilus* SDH−$NADP^+$ complex identified the putative $NADP^+$ binding site. The superposed $NADP^+$ with the *A. thaliana* SDH−shikimate complex produced a remarkable simulation of the ternary complex (Figure 4). C4 of the nicotinamide ring is within 3 Å of C3 of shikimate, a reasonable distance for hydride transfer. This observation further supports our findings about the location of the SDH active site. The SDH domain also cocrystallized with a sulfate ion. The sulfate ion interacts mostly with the backbone nitrogens of Glu 386, Lys 385, and Gly 463, of which Gly 463 belongs to the diphosphate binding loop motif, GXG-GXX, where X is usually a small hydrophobic or polar residue, and glycines 460, 462, and 463 constitute the G-motif.

Mechanistic Analysis of A. thaliana SDH Yielding the Kinetic Properties of Wild-Type and Active Site Mutants

Kinetic Parameters for Shikimate and $NADP^+$. Kinetic analysis of the SDH domain indicated that it belongs to the AroE class of shikimate dehydrogenases. The K_m values for shikimate and $NADP^+$ are 685 ± 36 and 131 ± 9 μM, respectively; both are similar to previously reported values for the AroE enzyme from other plant species (*30*−*33*), and the k_{cat} is 428 ± 10 s^{-1} (Table 3).

Analysis of Potential Catalytic Groups in the SDH Active Site. Lys 385 and Asp 423 are conserved in all SDHs and hydrogen bond to the C3 hydroxyl of shikimate (Figure 4). Since they are the only ionizable residues closest to the C3 hydroxyl of shikimate, we proposed that they are involved in proton transfer during catalysis.

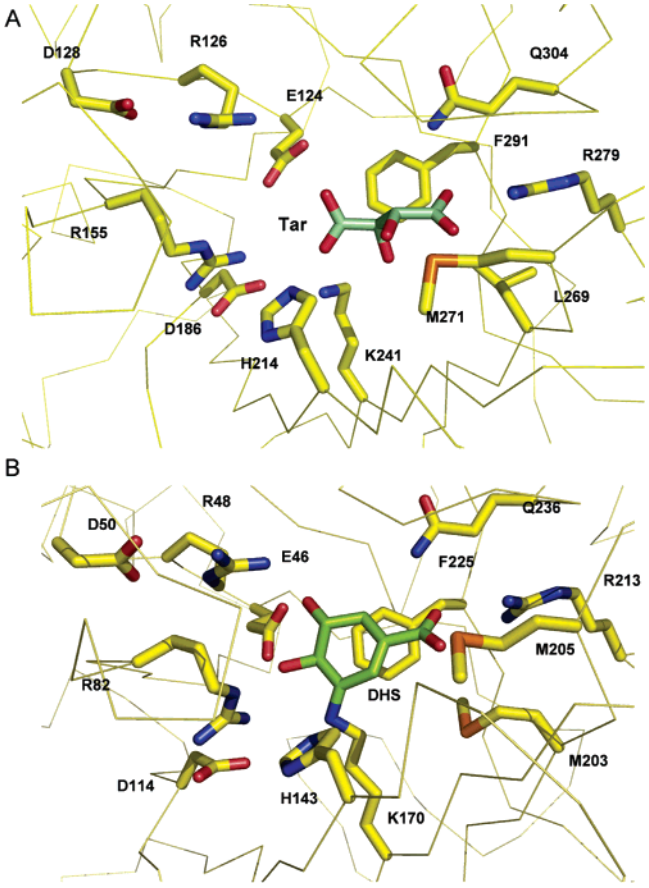

FIGURE 3: *A. thaliana* DHQ−tartrate and *S. typhi* DHQ−dehydroshikimate complexes showing the high degree of conservation of the active site architecture. (A) *A. thaliana* DHQ active site bound with tartrate. The tartrate−DHQ interactions mimic those seen in the *S. typhi* DHQ−dehydroshikimate structure with nearly all of the active site residues being identical. (B) *S. typhi* DHQ active site of the covalently bound dehydroshikimate. Some of the featured interactions include the conserved binding group, Arg 213, the catalytic base, His 143, and Lys 170 which forms an imine intermediate with C3 of dehydroshikimate.

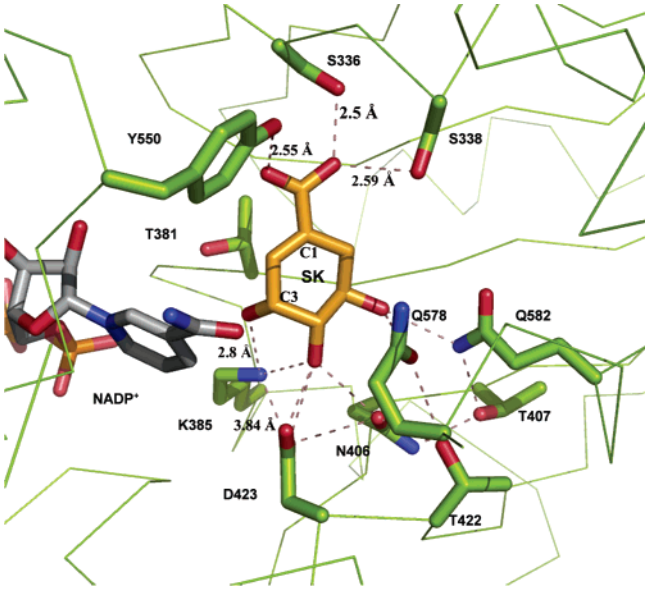

FIGURE 4: *A. thaliana* SDH ternary complex. The shikimate molecule (SK) is bound to the *A. thaliana* structure, and the $NADP^+$ molecule was positioned as a consequence of superimposition of the *A. thaliana* (shikimate) and *T. thermophilus* ($NADP^+$) active sites. The $NADP^+$ nictonamide ring is positioned for hydride transfer from C3 of shikimate to C4 of $NADP^+$, and Lys 385 and Asp 423 are positioned to mediate proton transfer from the C3 hydroxyl group. Other residues of interest include those which interact with the C1 carboxylate (Ser 336, Ser 338, and Tyr 550) as well as those surrounding the C4 and C5 hydroxyl groups (Asn 406, Gln 578, and Gln 582). For clarity, distances in angstroms are highlighted for key interactions. Shikimate C1 and C3 ring atoms are labeled.

A mutation of either lysine or aspartate to an alanine removes the charge effect and thus the ability of either group to participate in proton extraction. However, alanine is much smaller than lysine and aspartate, with respect to their van der Waals volume (67, 135, and 91 $Å^3$, respectively), which could induce a conformational effect on the protein. As such, a reasonably conservative mutation to an asparagine (96 $Å^3$) was also conducted. The Lys385Ala mutant showed a dramatic reduction (3×10^4-fold reduction) in turnover rate (0.013 ± 0.002 s^{-1}) with relatively minor effects on the K_m for shikimate (263 ± 85 μM, a 2.6-fold reduction) and for $NADP^+$ (17 ± 5 μM, a 7.7-fold reduction). The substitution with asparagine also resulted in a marked reduction (7×10^4-fold) in the k_{cat} (0.063 ± 0.002 s^{-1}), while the shikimate and $NADP^+$ K_m values of 470 ± 56 and 53 ± 6.4 μM, respectively, were similar to those of the wild-type enzyme (Table 3).

The Asp423Ala mutant had no measurable activity even at high enzyme (35 μM) and substrate (5 mM) concentrations. The concentration of the wild-type enzyme in the assay is usually between 40 and 100 nM; therefore, an at least 500-fold higher protein concentration was used in the assay for the mutant. The Asp423Asn mutant partially restored enzyme activity; however, we still observed a large reduction (3.5×10^3-fold) in the turnover rate (0.121 ± 0.001 s^{-1}) with respect to the wild-type enzyme. The K_m values for shikimate (555 ± 59 μM) and $NADP^+$ (79 ± 5 μM) were not affected. Interestingly, the turnover rate for the double mutant, Lys385Asn/Asp423Asn, was similar to that of either Lys385Asn or Asp423Asn (Table 3). These results indicate that both groups are important for catalysis. Furthermore, in the structure, these two groups form an ion pair; therefore, we envisioned that Lys 385 and Asp 423 are functioning as a catalytic dyad where the mutation of one residue results in the loss of functionality of the other.

Analysis of Potential Binding Groups in the SDH Active Site. The crystal structure of *A. thaliana* SDH indicated that Ser 336, Ser 338, and Tyr 550 are within hydrogen bonding distance of the C1 carboxylate of shikimate and thus may be important for binding shikimate. The Ser336Ala mutant had a pronounced effect on shikimate binding. We observed a 13-fold increase in the K_m for shikimate (8.7 ± 2.4 mM), with relatively no effect on the k_{cat} (140 ± 28 s^{-1}). The Ser338Ala mutant, on the other hand, affected substrate binding and catalysis. The mutant showed a 10-fold decrease in k_{cat} (33.2 ± 0.9 s^{-1}) in conjunction with a 9-fold increase in K_m (6.2 ± 9.3 mM). The effects of either a Tyr550Phe or a Tyr550Ala mutation were also 2-fold in magnitude. For each mutant, a 100-fold decrease in k_{cat} was observed with a doubling of the K_m (Table 3). The mutagenesis analysis of the above-mentioned groups indicates that Ser 336 plays an important role in binding shikimate; Ser 338 could help in binding and orienting shikimate, and Tyr 550 is important

Table 3: Steady-State Kinetic Profiles of the Wild Type and Active Site Mutants of the SDH Domain

	shikimate			$NADP^+$		
	k_{cat} (s^{-1})	K_M (μM)	k_{cat}/K_M ($\times 10^3$ s^{-1} M^{-1})	k_{cat} (s^{-1})	K_M (μM)	k_{cat}/K_M ($\times 10^3$ s^{-1} M^{-1})
wild type	428 ± 10	685 ± 36	624	399 ± 16	131 ± 9	3046
K385N	0.063 ± 0.002	470 ± 56	0.133	0.066 ± 0.002	53 ± 6	1.25
K385A	0.013 ± 0.002	263 ± 85	0.051	0.008 ± 0.001	17 ± 5	0.453
D423N	0.121 ± 0.001	555 ± 59	0.218	0.092 ± 0.001	79 ± 5	1.16
D423A	nd	nd		nd	nd	
K385N/D423N	0.043 ± 0.002	131 ± 31	0.324	0.036 ± 0.001	22 ± 5	1.62
wild type[a]				100 ± 4	118 ± 17	846
S336A	140 ± 28	8739 ± 2439	16.0	52.9 ± 3.2	152 ± 32	348
S338A	33.2 ± 0.9	6203 ± 926	5.35	11.2 ± 0.5	114 ± 24	98.2
Y550F	3.9 ± 0.2	1058 ± 124	3.67	3.11 ± 0.11	132 ± 14	23.6
Y550A	2.1 ± 0.2	1031 ± 270	2.04	1.86 ± 0.07	157 ± 20	11.8

[a] $NADP^+$ constants were calculated at a fixed, nonsaturating concentration of shikimate (250 μM).

for keeping shikimate in a catalytically competent geometry for the reaction.

Conformational Analysis of Wild-Type and Active Site Mutants

Circular Dichroism and Thermal Denaturation Studies. To determine if the differences in the K_m and k_{cat} values for the various active site mutants were not due to altered protein conformation, the far-ultraviolet spectra of wild-type Δ88DHQ-SDH and a selected set of mutants were determined and are presented in Figure 5A. All CD scans are similar, indicating that there are no global conformational changes to the mutant proteins. Thermal denaturation studies were also conducted to assess the overall stability of the mutants (Figure 5B). Thermal denaturation of the wild-type protein showed cooperative unfolding with a melting temperature of 60 °C. All of the active site mutants that were analyzed exhibited a denaturation profile similar to that of the wild type, and their melting temperatures did not deviate dramatically from that of the wild-type enzyme (Figure 5B). The CD and thermal denaturation studies, therefore, indicated that the observed differences in the kinetic parameters of the SDH active site mutants were not due to any global conformational changes.

Mode of Substrate Selectivity for the SDH

The structure of the *A. thaliana* SDH in complex with shikimate allows us to investigate the mode of substrate discrimination among the three classes of the SDH enzyme. Superimposition of the available AroE structures revealed a highly conserved active site among these enzymes (Figure 6A). All of the residues that interact with shikimate in the *A. thaliana* SDH superimpose with the other AroEs' active site residues. Superimposition of the SDH−shikimate structure with the existing YdiB class enzyme, which utilizes quinate as a natural substrate, revealed that only a single residue deviates from the highly conserved active site. Thr 381 is replaced with a serine in the YdiB enzyme (Figure 6B). In contrast, the comparison of the SDH−shikimate structure with the SDH-L class, whose natural substrate is unknown, revealed a number of deviations from the conserved active site seen in the AroE class. First, like YdiB, SDH-L also possesses a serine in place of Thr 381; second, only the Ser 336 position of AroE is conserved in SDH-L (Ser 17), whereas a glycine and an alanine replace Ser 338 and Tyr 550, respectively. Third, there are two additional serines in SDH-L, deeper in the substrate-binding pocket (Ser 11 and Ser 13, Figure 6C), which are unique to SDH-L. These results suggest that the SDH-L enzyme may accept a derivatized shikimate, a molecule with a more extended or a larger attachment at the C1 position of the shikimate ring.

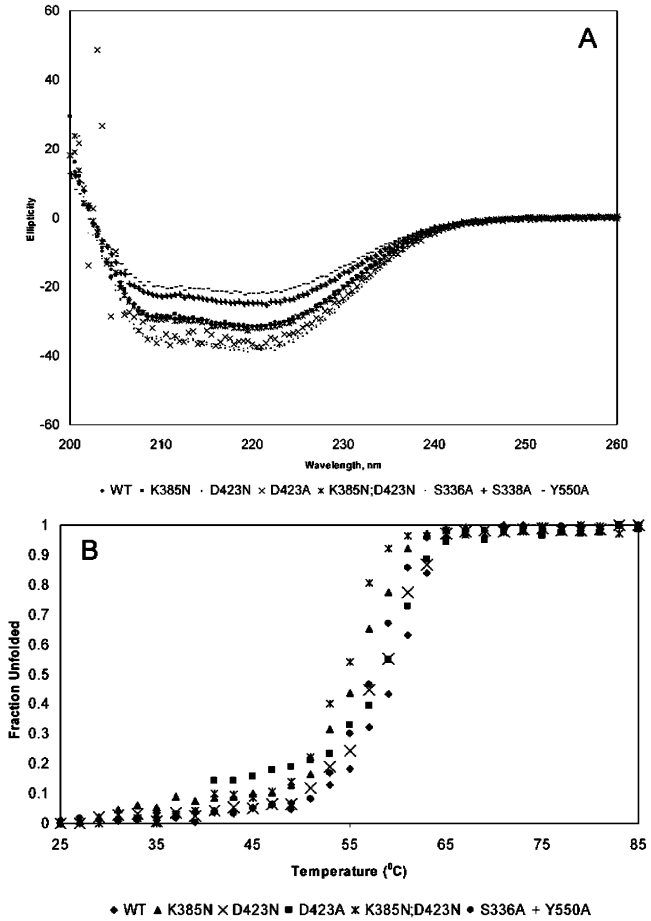

FIGURE 5: Circular dichroism scans and thermal denaturation studies of the wild type and SDH active site mutants. (A) CD scans of the wild type and mutants show identical profiles. (B) The thermal denaturation profiles of the SDH active site mutants do not deviate drastically from that of the wild-type enzyme.

DISCUSSION

The crystal structure of Δ88DHQ-SDH consists of two functional domains, a DHQ domain and a SDH domain. The organization of secondary structures for the DHQ domain is typical of a type I DHQ enzyme with the exception of a missing β hairpin which caps one opening of the β barrel.

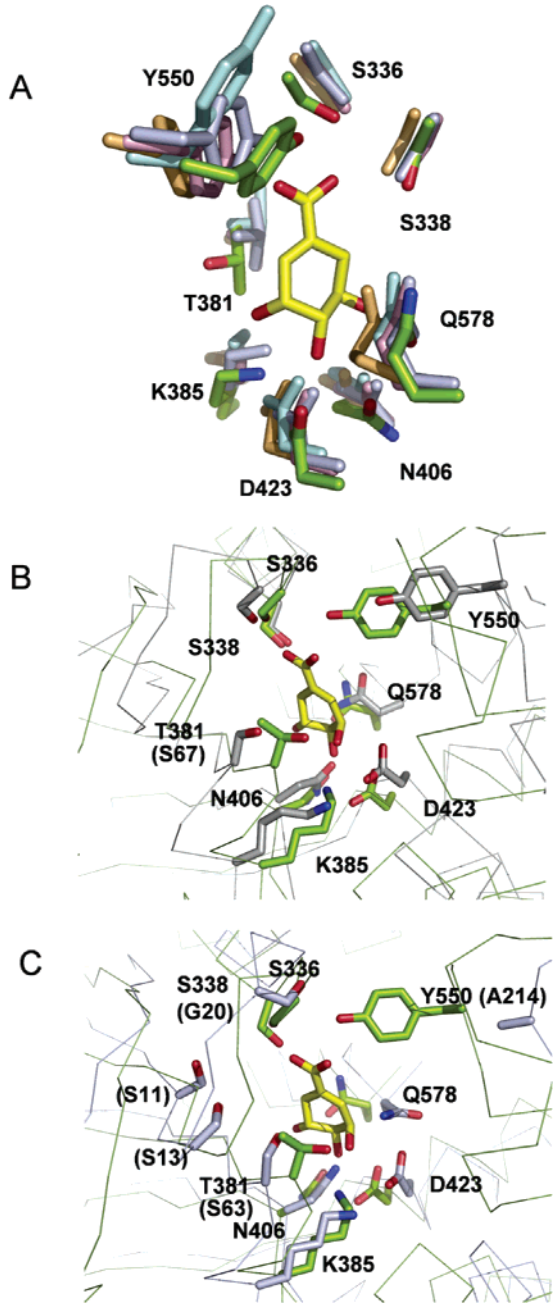

FIGURE 6: Superimposition of the *A. thaliana* SDH-shikimate active site with the AroE, YdiB, and SDH-L classes of dehydrogenases. (A) The superimposition of the AroE class shows total conservation of the residues interacting with shikimate; these residues include Ser 336 which was shown to be critical for binding and the catalytic residues, Lys 385 and Asp 423: green for *A. thaliana*, purple for *E. coli*, teal for *H. influenzae*, pink for *T. thermophilus*, and orange for *M. jannaschii*. (B) YdiB from *E. coli* (gray) also shows a highly conserved active site with the exception of a substitution of the equivalent Thr 381 with a serine (S63). (C) SDH-L (purple) shows less conservation by possessing an alanine (A214) instead of a tyrosine at position 550 and a glycine (G20) instead of a serine at position 338. SDH-L also possesses additional serines (S11 and S13) which are not present in the AroE or YdiB class.

The crystallization of tartrate in the protein identifies a number of conserved active site groups which have been implicated in the catalytic mechanism of the DHQ reaction. This observation strongly supports the notion of a conserved catalytic mechanism between the *S. typhi* and *A. thaliana* DHQ enzymes.

The organization of secondary structures for the *A. thaliana* SDH functional domain is similar to those of the other SDH structures. The overall topology is conserved among the shikimate dehydrogenase family. Cocrystallization with shikimate in the SDH domain resulted in the identification of active site residues that are involved in important interactions with the substrate. The role of these active site residues was investigated by site-directed mutagenesis and kinetics analysis. Mutation of either Lys 385 or Asp 423 had a direct impact on the turnover rate; we observed a more than 1000-fold reduction in k_{cat} and very little effect on the Michaelis constant (K_m) for both shikimate and $NADP^+$. Incidentally, a reduction in k_{cat} that was similar in magnitude was observed by mutating either residue, indicating that they are both important catalytic groups. Subsequently, the double mutant, Lys385Asn/Asp423Asn, did not impose any further reduction on k_{cat} compared to that already observed with either the Lys 385 or the Asp 423 single mutant. These findings are consistent with Lys 385 and Asp 423 functioning as a catalytic dyad; that is, the loss of either residue produces an inactive enzyme. This finding is supported by our observation with the crystal structure which indicated that they are involved in ionic interactions with shikimate.

Despite the high degree of conservation of active site architecture between the AroE and YdiB classes (Figure 6B), the site-directed mutagenesis study conducted by Linder et al. on *E. coli* YdiB suggests that the equivalent lysine (Lys 71) and aspartate (Asp 107) residues are instead key binding rather than catalytic groups. The authors proposed that their results do not support a role for general acid−base catalysis for the YdiB enzyme. This is in contrast to our findings which demonstrated that Lys 385 and Asp 423 are functioning as a catalytic dyad in the *A. thaliana* SDH reaction. It is of extreme interest to observe such marked differences in kinetic parameters for the two functional classes of SDH enzymes, although they catalyze similar reactions and they both accept shikimate as a substrate. Our findings are consistent with work done on SDH-L from *Haemophilus influenzae* which demonstrated that its activity was reduced to an undetectable level when either Lys 67 or Asp 103 was mutated (*11*). Furthermore, Dennis and Balinksy (*34*) investigated the effects of various shikimate analogues on the kinetic properties of *Pisum sativum* AroE, which revealed that the C1 carboxylate and C4 hydroxyl groups of shikimate were important for binding. These kinetics studies are further corroborated by the *A. thaliana* AroE−shikimate complex which identified residues proximal to the C1 position (Ser 336, Ser 338, and Tyr 550) and the C4 position, Asn 406, whereas the catalytic dyad, Lys 385−Asp 423, is proximal to the C3 position of shikimate (Figure 4).

Mutagenesis of either Ser 336 or Ser 338 had a pronounced effect on shikimate binding; additionally, the Ser 338 mutant also resulted in 10-fold reduction in the turnover rate. Ser 336 is highly conserved among the SDHs and is positioned to interact with the C1 carboxylate of shikimate. These results are consistent with Ser 336 being a key binding group for the SDH class of proteins. Ser 338 has dual roles; it is involved in binding and also in positioning the substrate for catalysis. Tyr 550 on the other hand is predominantly involved in positioning the substrate since we see a >100-fold reduction in the level of binding of shikimate to the E−$NADP^+$ complex but a weaker effect on the turnover rate.

Scheme 2: Three Possible Modes of Substrate Channeling between DHQ and SDH[a]

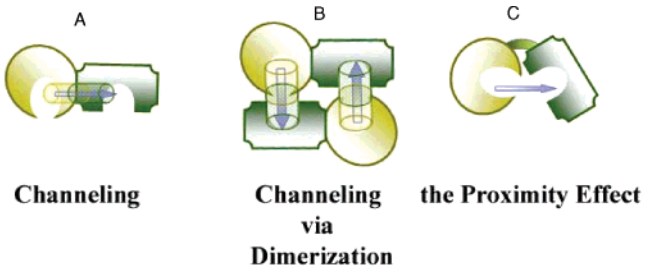

[a] (A) In model 1, a physical channel is formed by residues within the bifunctional enzyme linking the two active sites. (B) In model 2, upon dimerization, a physical channel is formed by residues contributed from each monomer. (C) In model 3, the active sites of each catalytic domain are positioned proximal to each other to increase the effective concentration of the intermediate, dehydroshikimate. Cylinders represent tunnels formed by residues from each catalytic domain.

The superimposition permits the first comprehensive study of the mode of substrate binding for this family of dehydrogenases. A comparison of all three classes of SDH with the *A. thaliana* SDH−shikimate complex indicated that differences in the active site architecture occur predominantly around the C1 carboxylate. Our mutagenesis data for the Ser 336, Ser 338, and Tyr 550 residues indicated that interactions with the C1 carboxylate are important for substrate binding and orientation. Studies with structural analogues of shikimate further support this observation (*34*). We therefore envision a mode for substrate specificity which is dictated by the variation of residues in this area of the active site.

Bifunctional enzymes play important roles in regulating the partition of intermediates or reactive species at branch points in metabolic pathways to ensure sufficient production of a desired compound(s). The identification of only a small number of bifunctional enzymes in plants further highlights their importance at these positions in metabolic pathways. The advantages of such protein fusions include enhanced coordinated gene expression and/or increased flux efficiency (*15*). In the case of DHQ-SDH, metabolic control is the likely reason for the fusion protein since this enzyme is found at the branch point for quinate biosynthesis. Dehydroquinate and dehydroshikimate, the substrates for DHQ and SDH, can be partitioned toward quinate metabolism.

The bifunctional enzyme DHQ-SDH plays an important role in controlling the partitioning of metabolites to the quinate biosynthetic pathway by channeling dehydroshikimate from the DHQ to the SDH active site (*15*). Kinetic data for plant bifunctional DHQ-SDH support this model by demonstrating that the turnover rate for SDH is ~9 times faster than that of DHQ (*33*). In contrast, the turnover rates for the monofunctional DHQ and SDH enzymes are similar, 142 and 237 s^{-1}, respectively (*12*, *27*). There are three current models via which metabolite channeling could occur through bifunctional DHQ-SDH, shown in Scheme 2. Model 1 involves a physical channel, which links the DHQ site to the SDH active site. In this model, dehydroshikimate will be directly routed to the SDH site without being released to the cellular milieu. This physical organization is observed in a number of bifunctional enzymes, including imidazole glycerol phosphate synthase (*35*) and glutamine phosphoribosylpyrophosphate amidotransferase (*36*). However, we did not observe a physical tunnel in the DHQ-SDH crystal structure. Model 2 involves the formation of a physical tunnel following the dimerization of an enzyme as observed for carbamoyl phosphate synthetase whose molecular tunnel is formed upon dimerization of the two enzyme subunits (*37*). DHQ-SDH is monofunctional in solution as determined by gel filtration studies (data not shown). The structure of DHQ-SDH was determined as a monomer in the asymmetric unit; however, crystal packing revealed that the symmetry-related molecule produced a dimer in which the DHQ domain formed pairwise interactions with the SDH domain. However, this organization of the enzyme in the crystal resulted in a staggered intermonomer arrangement of the DHQ and SDH active sites. We do not feel that this staggered arrangement of the active sites in the dimer is optimal for metabolic channeling. In addition, we did not observe a physical pathway which could facilitate transfer of dehydroshikimate to the SDH site. However, we investigated this model further by conducting gel filtration studies in the presence of tartrate and shikimate separately. We observed no shift in the physical state of DHQ-SDH in the presence of tartrate or shikimate; the protein remained monomeric in solution, thus eliminating the dimerization model as a mode for metabolite channeling in the DHQ-SDH enzyme. Model 3 illustrates a mode for increasing metabolic flux by bringing two reactive sites into the proximity of each other, thus simplifying the pathway via which the substrate is sequestered. This mechanism for improving catalytic efficiency has been suggested for hydroxymethyl-dihydropterin-pyrophosphokinase-dihydropteroate-synthase and for DHQ-SDH (*15*, *38*). The crystal structure of Δ88DHQ-SDH indicates that model 3 is the most likely mechanism for increased metabolic flux through the shikimate pathway. The enzyme adopts a concave architecture (Figure 2B) which places the two active sites in proximity and facing each other. In this model, the concave architecture of the enzyme would enhance the transfer of dehydroshikimate to the SDH site by increasing the local, effective concentration of dehydroshikimate at the SDH site. If these two enzymes are physically separated, the effective concentration at the SDH site would be dependent on their relative positions in the cell, on the diffusion rate of dehydroshikimate to the SDH site, and on the demands for dehydroshikimate by competing enzymes in the cell. The face-to-face organization of the DHQ and SDH active sites would therefore ensure this increased efficiency by providing a direct route for dehydroshikimate to the SDH site.

The structure of *A. thaliana* DHQ-SDH represents the first bifunctional shikimate pathway enzyme; moreover, it is the first report of a plant structure for this pathway. The structure of the cocomplexes, DHQ−tartrate−SDH−shikimate−(superposed $NADP^+$), provides a unique opportunity to understand the catalytic and regulatory mechanisms of this enzyme. We have now established that *A. thaliana* DHQ catalyzes the dehydration of dehydroquinate via a mechanism consistent with the type I DHQ enzyme. The structure of SDH in complex with shikimate allowed us to dissect the role of active site residues in substrate binding and catalysis. The active site is conserved among the three classes of SDHs; variation from this conserved architecture confers substrate specificities. The arrangement of the two functional domains, DHQ and SDH, is such that substrate transfer from one site to the next is maximized through the proximity effect. The

crystal structure of this bifunctional enzyme with its substrate and substrate analogue advances our understanding of drug and herbicide design against the shikimate pathway.

ACKNOWLEDGMENT

We thank Martin McMillan from the NSLS for collecting the X-ray data and Vivian Saridakis for her assistance in the preparation of the manuscript.

REFERENCES

1. Schonbrunn, E., Eschenburg, S., Shuttleworth, W. A., Schloss, J. V., Amrhein, N., Evans, J. N., and Kabsch, W. (2001) Interaction of the herbicide glyphosate with its target enzyme 5-enolpyruvylshikimate 3-phosphate synthase in atomic detail, *Proc. Natl. Acad. Sci. U.S.A. 98*, 1376−80.
2. Priestman, M. A., Healy, M. L., Funke, T., Becker, A., and Schonbrunn, E. (2005) Interaction of the herbicide glyphosate with its target enzyme 5-enolpyruvylshikimate 3-phosphate synthase in atomic detail, *FEBS Lett. 579*, 5773−80.
3. Owen, M. D., and Zelaya, I. A. (2005) Herbicide-resistant crops and weed resistance to herbicides, *Pest Manage. Sci. 61*, 301−11.
4. Meganathan, R. (2001) Ubiquinone biosynthesis in microorganisms, *FEMS Microbiol. Lett. 203*, 131−9.
5. Humphreys, J. M., and Chapple, C. (2002) Rewriting the lignin roadmap, *Curr. Opin. Plant Biol. 5*, 224−9.
6. Herrmann, K. M. (1995) The shikimate pathway as an entry to aromatic secondary metabolism, *Plant Physiol. 107*, 7−12.
7. Gourley, D. G., Shrive, A. K., Polikarpov, I., Krell, T., Coggins, J. R., Hawkins, A. R., Isaacs, N. W., and Sawyer, L. (1999) The two types of 3-dehydroquinase have distinct structures but catalyze the same overall reaction, *Nat. Struct. Biol. 6*, 521−5.
8. Nichols, C. E., Lockyer, M., Hawkins, A. R., and Stammers, D. K. (2004) Crystal structures of *Staphylococcus aureus* type I dehydroquinase from enzyme turnover experiments, *Proteins 56*, 625−8.
9. Nichols, C. E., Hawkins, A. R., and Stammers, D. K. (2004) Structures of the 'open' form of *Asperigullus nidulans* 3-dehydroquinate synthase of 1.7 Å resolution from crystals grown following enzyme turnover, *Acta Crystallogr. D60*, 971−3.
10. Frederickson, M., Roszak, A. W., Coggins, J. R., Lapthorn, A. J., and Abell, C. (2004) (1R,4S,5R)-3-Fluoro-1,4,5-trihydroxy-2-cyclohexene-1-carboxylic acid: The fluoro analogue of the enolate intermediate in the reaction catalyzed by type II dehydroquinases, *Org. Biomol. Chem. 2*, 1592−6.
11. Singh, S., Korolev, S., Koroleva, O., Zarembinski, T., Collart, F., Joachimiak, A., and Christendat, D. (2005) Crystal structure of a novel shikimate dehydrogenase from *Haemophilus influenzae*, *J. Biol. Chem. 280*, 17101−8.
12. Michel, G., Roszak, A. W., Sauve, V., Maclean, J., Matte, A., Coggins, J. R., Cygler, M., and Lapthorn, A. J. (2003) Structures of shikimate dehydrogenase AroE and its paralog YdiB. A common structural framework for different activities, *J. Biol. Chem. 278*, 19463−72.
13. Padyana, A. K., and Burley, S. K. (2003) Crystal structure of shikimate 5-dehydrogenase (SDH) bound to NADP: Insights into function and evolution, *Structure 11*, 1005−13.
14. Ye, S., Von Delft, F., Brooun, A., Knuth, M. W., Swanson, R. V., and McRee, D. E. (2003) The crystal structure of shikimate dehydrogenase (AroE) reveals a unique NADPH binding mode, *J. Bacteriol. 185*, 4144−51.
15. Moore, B. (2004) Bifunctional and moonlighting enzymes: Lighting the way to regulatory control, *Trends Plant Sci. 9*, 221−8.
16. Maher, E. A., Bate, N. J., Ni, W., Elkind, Y., Dixon, R. A., and Lamb, C. J. (1994) Increased disease susceptibility of transgenic tobacco plants with suppressed levels of preformed phenylpropanoid products, *Proc. Natl. Acad. Sci. U.S.A. 91*, 7802−6.
17. Niggeweg, R., Michael, A. J., and Martin, C. (2004) Engineering plants with increased levels of the antioxidant chlorogenic acid, *Nat. Biotechnol. 22*, 746−54.
18. Boerjan, W., Ralph, J., and Baucher, M. (2003) Lignin biosynthesis, *Annu. Rev. Plant Biol. 54*, 519−46.
19. Cleland, W. W. (1979) Statistical analysis of enzyme kinetic data, *Methods Enzymol. 63*, 103−38.
20. Minor, W., Tomchick, D., and Otwinowski, Z. (2000) Strategies for macromolecular synchrotron crystallography, *Struct. Folding Des. 8*, R105−10.
21. Terwilliger, T. C., and Berendzen, J. (1999) Automated MAD and MIR structure solution, *Acta Crystallogr. D55* (Part 4), 849−61.
22. Terwilliger, T. C. (2000) Maximum-likelihood density modification, *Acta Crystallogr. D56* (Part 8), 965−72.
23. Perrakis, A., Morris, R., and Lamzin, V. S. (1999) Automated protein model building combined with iterative structure refinement, *Nat. Struct. Biol. 6*, 458−63.
24. Jones, T. A., Zou, J. Y., Cowan, S. W., and Kjeldgaard, M. (1991) Improved methods for building protein models in electron density maps and the location of errors in these models, *Acta Crystallogr. A47* (Part 2), 110−9.
25. Brunger, A. T., Adams, P. D., Clore, G. M., DeLano, W. L., Gros, P., Grosse-Kunstleve, R. W., Jiang, J. S., Kuszewski, J., Nilges, M., Pannu, N. S., Read, R. J., Rice, L. M., Simonson, T., and Warren, G. L. (1998) Crystallography & NMR system: A new software suite for macromolecular structure determination, *Acta Crystallogr. D54* (Part 5), 905−21.
26. Esnouf, R. M. (1997) An extensively modified version of MolScript that includes greatly enhanced coloring capabilities, *J. Mol. Graphics Modell. 15*, 132−4, 112−3.
27. Leech, A. P., James, R., Coggins, J. R., and Kleanthous, C. (1995) Mutagenesis of active site residues in type I dehydroquinase from *Escherichia coli*. Stalled catalysis in a histidine to alanine mutant, *J. Biol. Chem. 270*, 25827−36.
28. Kleanthous, C., Reilly, M., Cooper, A., Kelly, S., Price, N. C., and Coggins, J. R. (1991) Mutagenesis of active site residues in type I dehydroquinase from *Escherichia coli*. Stalled catalysis in a histidine to alanine mutant, *J. Biol. Chem. 266*, 10893−8.
29. Bello, C. G., Harris, J. M., Manthey, M. K., Coggins, J. R., and Abell, C. (2000) Irreversible inhibition of type I dehydroquinase by substrates for type II dehydroquinase, *Bioorg. Med. Chem. Lett. 10*, 407−9.
30. Balinsky, D., Dennis, A. W., and Cleland, W. W. (1971) Kinetic and isotope-exchange studies on shikimate dehydrogenase from *Pisum sativum*, *Biochemistry 10*, 1947−52.
31. Nandy, M., and Ganguli, N. C. (1961) Studies on 5-dehydroshikimic reductase from mung bean seedlings (*Phaseolus aureus*), *Arch. Biochem. Biophys. 92*, 399−408.
32. Sanderson, G. W. (1966) 5-Dehydroshikimate reductase in the tea plant (*Camellia sinensis* L.). Properties and distribution, *Biochem. J. 98*, 248−52.
33. Schmidt, C., Grundemann, D., Groth, G., Muller, B., Henning, H., and Schultz, G. (1991) Shikimate Pathway in Non-photosynthetic Tissues. Identification of Common Enzymes and Partial Purification of Dehydroquinate Hydrolyase-Shikimate Oxidoreductase and Chorismate Mutase from Roots, *J. Plant Physiol. 138*, 51−6.
34. Dennis, A. W., and Balinsky, D. (1972) The effect of pH on the kinetic parameters of shikimate dehydrogenase from *Pisum sativum*, *Int. J. Biochem. 3*, 93−102.
35. Chaudhuri, B. N., Lange, S. C., Myers, R. S., Chittur, S. V., Davisson, V. J., and Smith, J. L. (2001) Crystal structure of imidazole glycerol phosphate synthase: A tunnel through a $(\beta/\alpha)_8$ barrel joins two active sites, *Structure 9*, 987−97.
36. Krahn, J. M., Kim, J. H., Burns, M. R., Parry, R. J., Zalkin, H., and Smith, J. L. (1997) Coupled formation of an amidotransferase interdomain ammonia channel and a phosphoribosyltransferase active site, *Biochemistry 36*, 11061−8.
37. Thoden, J. B., Holden, H. M., Wesenberg, G., Raushel, F. M., and Rayment, I. (1997) Structure of carbamoyl phosphate synthetase: A journey of 96 Å from substrate to product, *Biochemistry 36*, 6305−16.
38. Lawrence, M. C., Iliades, P., Fernley, R. T., Berglez, J., Pilling, P. A., and Macreadie, I. G. (2005) The three-dimensional structure of the bifunctional 6-hydroxymethyl-7,8-dihydropterin pyrophosphokinase/dihydropteroate synthase of *Saccharomyces cerevisiae*, *J. Mol. Biol. 348*, 655−70.

BI060366+